Erciyes Üniversitesi
Enginoscope Dergisi
Cilt 1, Sayı 2, 2025

Erciyes University
Enginoscope Journal
Volume 1, Issue 2, 2025

Analysis of the Internal Ballistic Process of a 9x19 mm Pistol Barrel Using the Finite Element Method and Experimental Validation

Burak ÖZCAN*[1], MEHMET SEYİS[2], ULVİ ŞEKER[3], Abdullah KURT[3]

*[1] Gazi University, Graduate School of Natural and Applied Sciences, ANKARA
[2] North logistic and international trade LLC - Orlando / Florida
[3] Gazi University, Faculty of Technology, Department of Manufacturing Engineering, ANKARA

(Alınış / Received: 17.06.2025, Kabul / Accepted: 25.07.2025, Online Yayınlanma / Published Online: 31.07.2025)

Keywords
Finite Element Analysis,
Interior Ballistic,
JWL Model,
Gun Barrel.

Abstract: In this study, the barrel and bullet geometries of a 9x19 mm calibre pistol system were modelled using the finite element method, and the thermo-mechanical behaviour developing as a result of the internal ballistic process after firing was analysed numerically. AISI 4340 and brass materials were assigned to the barrel and bullet used in the weapon system, respectively; the sensitivity of material behaviour to high temperature and strain rate was represented by the Johnson-Cook (JC) model. The internal ballistic pressure-time data were obtained using the Vallier-Heydenreich equations, and the stress, plastic deformation, temperature, and bullet exit velocity values developing between the bullet and the barrel over time were analysed in the Explicit Dynamics module of the Ansys Workbench software. The analysis results were validated with experimental data obtained from the actual firing rig; it was determined that the obtained bullet exit velocity showed a deviation of 1.82% from the experimental measurement. Additionally, the plastic deformation occurring in the bullet core after firing was compared with the bullet geometry scanned after actual firings, and the physical accuracy of the numerical model was evaluated numerically. The study demonstrates that validated numerical models are an effective tool for optimising ballistic design processes by reducing the need for prototypes.

9x19 mm Tabanca Namlusunun İç Balistik Sürecinin Sonlu Elemanlar Yöntemiyle Analizi ve Deneysel Doğrulama

Anahtar Kelimeler
Sonlu Elemanlar Analizi,
İç Balistik,
JWL Modeli,
Tabanca Namlusu.

Öz: Bu çalışmada, 9x19 mm kalibreye sahip bir tabanca sistemine ait namlu ve mermi geometrileri sonlu elemanlar yöntemi ile modellenmiş ve ateşleme sonrası iç balistik sürece bağlı olarak gelişen termo-mekanik davranışlar sayısal olarak analiz edilmiştir. Silah sisteminde kullanılan namlu ve mermi için sırasıyla AISI 4340 ve pirinç malzeme atanmış; malzeme davranışlarının yüksek sıcaklık ve şekil değiştirme hızına duyarlılığı Johnson-Cook (JC) modeli ile temsil edilmiştir. İç balistik basınç-zaman verileri, Vallier-Heydenreich denklemleri yardımıyla elde edilmiş ve zamana bağlı olarak mermi ile namlu arasında gelişen gerilme, plastik deformasyon, sıcaklık ve mermi çıkış hızı değerleri Ansys Workbench yazılımının Explicit Dynamics modülünde analiz edilmiştir. Analiz sonuçları, gerçek atış düzeneğinde elde edilen deneysel verilerle doğrulanmış; elde edilen mermi çıkış hızının deneysel ölçümle %1,82 oranında bir sapma gösterdiği belirlenmiştir. Ayrıca, ateşleme sonrası mermi çekirdeğinde meydana gelen plastik deformasyon, gerçek atışlar sonrası taranmış olan mermi geometrisi ile karşılaştırılmış ve sayısal modelin fiziksel doğruluğu sayısal olarak değerlendirilmiştir. Çalışma, doğrulanmış sayısal modellerin, prototip gereksinimini azaltarak balistik tasarım süreçlerini optimize etmede etkili bir araç olduğunu ortaya koymaktadır.

1. Introduction

In the design of firearm systems, the accurate modelling of the internal ballistic process is of critical importance in terms of firearm safety, effectiveness and service life. Internal ballistics is a highly complex physical process that involves the formation of explosive gases, the movement of the bullet within the barrel, bullet-barrel interaction, and the analysis of pressure, temperature, and stress distributions. The literature on this process is generally categorised into two main areas: experimental studies and numerical/computational analyses.

Experimental studies have mostly focused on directly measuring the pressure, temperature and stress values generated during firing and evaluating the effects of these physical events, such as wear, stress accumulation and barrel life. Morphy and Fisher [1] found that the high temperatures caused by explosive gases create wear on the barrel surface and demonstrated that carburisation provides protection against this effect. Özcan [2] evaluated the effect of surface treatments such as boronising, carburising, and boron carburising on the rifling geometry and demonstrated that the powder boronising method is applicable while maintaining surface quality. Değirmenci [3] conducted extensive firing tests with different ammunition configurations and successfully predicted the pressure distribution inside the barrel with high accuracy using velocity functions created from these data. Similarly, Piticari et al. [4] analysed the effect of muzzle attachments on vibration behaviour using high-speed imaging methods and demonstrated that these attachments can be accurately controlled. Zhang and Jia [5] combined experimental and mathematical modelling to evaluate the performance of automatic weapon mechanisms, including friction and buffer effects. This study provided important insights, particularly for the design of weapon systems with high firing rates.

Numerical studies, particularly using approaches such as the finite element method (FEM) and computational fluid dynamics (CFD), have focused on modelling the complex physical phenomena that occur during firing. Nelson and Ward [6] numerically investigated the effects of heat transfer on deformation in barrel walls; Huang [7] analysed the development of damage caused by explosions in a 105 mm cannon barrel using an energy density criterion and predicted the fragmentation that occurs at high pressure. Deng et al. [8] analysed the internal ballistic motion of a 5.56 mm rifle bullet using a non-linear discontinuous finite element method and used the pressure-time data obtained with the Vallier-Heydenreich method as input for the FEM model. The bullet exit velocity they obtained showed 95% agreement with experimental data. Sönmez [9] analysed the stresses caused by internal pressures obtained with different types of gunpowder in the barrel combustion chamber on a time-based basis. Öztürk [10] used the CFD approach to examine the effect of barrel design on recoil force and showed that optimised barrel geometry reduces this force. Akçay and Yükselen [11] calculated the convective heat transfer coefficients based on internal ballistics theory and analysed the temperature distribution of the rifle barrel over time. Danış [12] developed zero- and one-dimensional ballistic models and successfully predicted the muzzle velocity using analyses based on the Noble-Abel gas flow model. Gündüzer [13] analysed the model created using the internal ballistic data of the M101 gun barrel on the CATIA and ANSYS Workbench platforms and evaluated the stress distributions depending on the barrel wall thickness. Tawfik [14] numerically investigated the stability of the barrel under the effect of the bullet during firing using the Euler-Bernoulli rod model. Stiavnicky et al. [15] analysed the dynamic loads applied to the barrel during the firing of a NATO 5.56 mm bullet using LS-DYNA software and modelled the barrel vibration behaviour.

In general, internal ballistic analyses are conducted either experimentally or through simulation, but these two approaches are often considered separately. Experimental methods provide realistic data but can be time-consuming, costly, and dangerous, while numerical models are often limited by idealised assumptions and simplified material models. In our previous study, internal ballistic pressure-time data obtained using the Vallier-Heydenreich method were directly applied to the model in the Ansys Explicit Dynamics platform, and the bullet exit velocity was verified against experimental values. However, since these pressure loads did not directly model explosive effects, temperature distributions and gas-expansion behaviour could only be represented to a limited extent.

In this study, time-dependent pressure data obtained using the Vallier-Heydenreich equations were applied in the Explicit Dynamics module of Ansys Workbench software to model the internal ballistic process using the finite element method. Thus, fundamental quantities such as stress, plastic deformation, temperature distribution, and bullet exit velocity were calculated during the interaction between the bullet and the barrel. The calculated bullet exit velocity was compared with experimental shots conducted in a standard ballistic test setup to evaluate the accuracy of the model, and it was observed that the analysis results were in high agreement with the experimental data. Additionally, the plastic deformation geometry obtained in the bullet core as a result of the simulations was quantitatively compared with the scanned bullet form after the actual firing, and the physical reality of the numerical model was verified. In this regard, the study enables reliable predictions to be obtained in the ballistic

design process by bringing together experimental and numerical data in a holistic approach and makes a meaningful contribution to empirical-based analysis approaches in the literature.

2. Material and Method

In this section, the properties of the materials used and the methods used within the scope of the study will be explained.

2.1. Material

The barrel and bullet parameters examined in the study are given in Table 1.

Table 1. Barrel and bullet parameters

Calibre	9 mm
Barrel length	86
Number of rifling grooves	6 (right)
Powder charge	0.325 g
Bullet weight	8 ± 0.075 g
Bullet jacket material	Brass
Bullet core material	Lead-Antimony Alloy
Muzzle velocity	350 m/s
Barrel material	AISI 4340

The Johnson-Cook material model parameters for the barrel and bullet are given in Table 2 [16].

Table 2. JC parameters of materials

Material	**AISI 4340 (Barrel)**	**CUOFHC2 (Bullet)**
A (MPa)	792	90
B (MPa)	510	292
n	0.26	0.31
C	0.014	0.025
m	1.03	1.09
T_r	27	27
T_m	1519.9	1082.9
$\dot{\bar{\varepsilon}}_0$ (s^{-1})	1	1

2.2. Methods

In this section, the methods used will be explained.

2.2.1. Explicit dynamic analysis

Within the scope of this study, the Explicit Dynamics analysis module of Ansys finite element software was used to solve internal ballistics problems. The explicit method can be effectively used to solve many problems, including high-frequency dynamic analyses, large deformations, geometric non-linearities, complex contact conditions, complex material behaviours (material damage, material failure), and the propagation of shock waves in solids and fluids [16].

2.2.2. Thermo-elastic-plastic material model

Within the scope of this study, due to the fact that the stress considered varies depending on temperature, strain and strain rate, it is necessary to accurately model the behaviour of the barrel and bullet material under high temperature/deformation and deformation rates. The Johnson-Cook (JC) material model is used to describe the behaviour of metals under high temperature/deformation and deformation rates. It is generally used to model material behaviour in high-speed impact, forming (rolling) and machining processes involving ductile metals. The JC model is particularly suitable for ductile metals subjected to high strain rates and temperatures, making it an appropriate choice for interior ballistic simulations involving materials like AISI 4340 and copper-based alloys.

$$\sigma = (A + B\epsilon^n)(1 + C\, ln\, \dot{\epsilon}^*)(1 - T^{*m}) \quad (1)$$

Here, σ represents the equivalent stress, ϵ is the plastic strain, A is the yield strength, B is the strain hardening coefficient, n is the strain hardening exponent, C is the strain rate sensitivity coefficient, and m is the thermal softening exponent.

$$[\dot{\epsilon}^* = \frac{\dot{\epsilon}}{\dot{\epsilon}_0}, \quad T^* = \frac{T - T_{\text{ref}}}{T_m - T_{\text{ref}}}] \quad (2)$$

Here, $\dot{\epsilon}^*$ denotes the dimensionless strain rate, T* is the homologous temperature, T_m is the melting temperature of the material, and T is the deformation temperature. $\dot{\epsilon}_0$ represents the reference strain rate, and T_{ref} is the reference deformation temperature. To obtain the constants in Eq. 1, stress-strain curves at different temperatures and strain rates are required [13].

2.2.3. Finite elements model

In explicit analyses, the mesh density directly affects the accuracy of the results and the solution time. Using a very dense solution mesh will increase the number of elements, resulting in a decrease in the characteristic length value of the elements. A decrease in characteristic length will reduce the time step value of the analysis and increase the solution time. However, if the solution mesh is not sufficiently dense, the finite element model will not be able to accurately reflect the problem.

The appearance of the original barrel model referenced is shown in Figure 1. However, a simplified geometric model was prepared for analysis, as shown in Figure 2. These simplifications were made to divide the geometric model into quadrilateral-based elements, reduce the number of elements, and increase the characteristic length. The aim was to reduce the analysis time. While making these simplifications, care was taken to ensure that the behaviour of the original model was not altered as much as possible. Additionally, in order to divide the barrel geometry into quadrilateral-based elements, it was divided into 12 separate parts along the lands and grooves helices, and each node point was merged with the others.

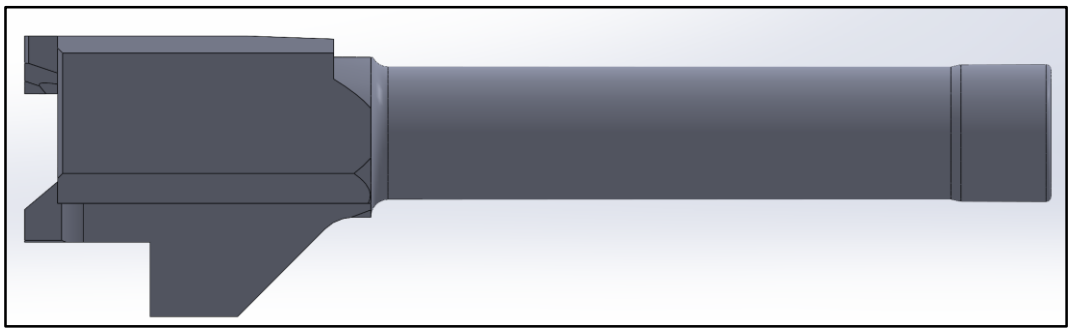

Figure 1. Original barrel geometry model.

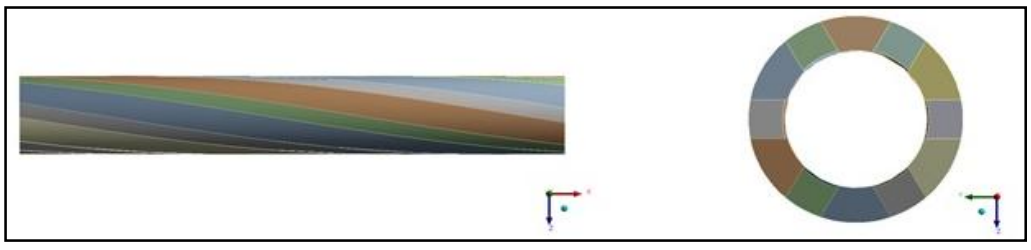

Figure 2. Simplified barrel analysis model.

In order to divide the bullet model into rectangular-based elements of similar dimensions, the tip of the bullet, which does not come into contact with the barrel during movement, was cut perpendicular to the direction of movement (Figure 3) and divided into eight pieces. The bullet volume is modelled as smaller in the analysis model, and to achieve the same mass, the bullet density is increased in the analysis model to maintain the same mass (8 g).

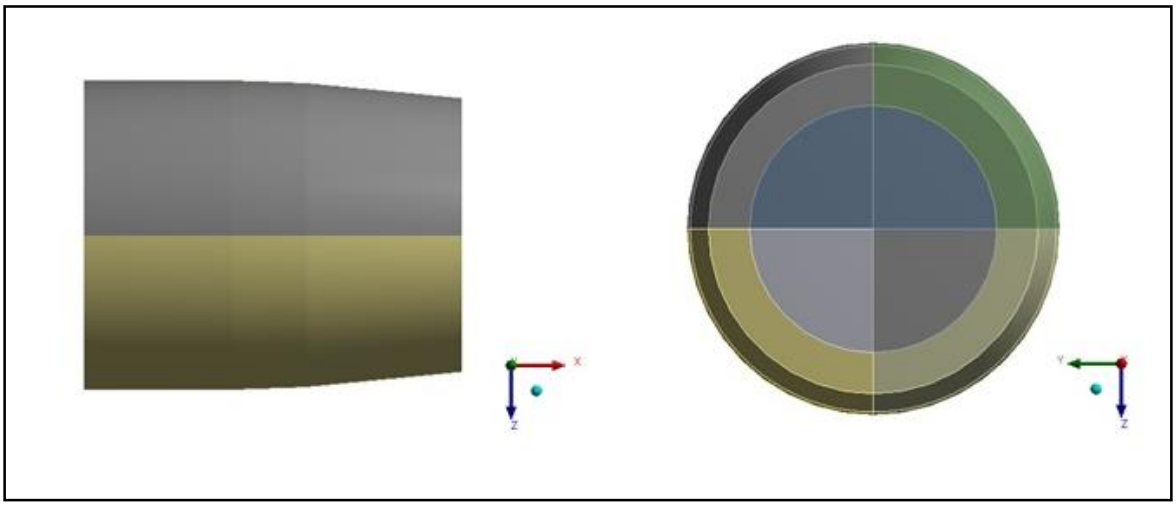

Figure 3. Simplified bullet analysis model.

The solution grids for the barrel and bullet geometry are shown in Figures 4 and 5, respectively. Only three-dimensional linear hexahedral elements, as shown in Figure 6, were used to create the solution grid. A total of 108,600 nodes were used in the solution grid for the barrel geometry and 109,968 nodes for the bullet geometry. Although the mesh was sufficiently refined, a mesh independence study was also conducted to ensure the reliability of the results. Meshes with varying element sizes were tested, and the resulting muzzle velocity values varied by less than 2.5%, confirming the numerical stability of the model.

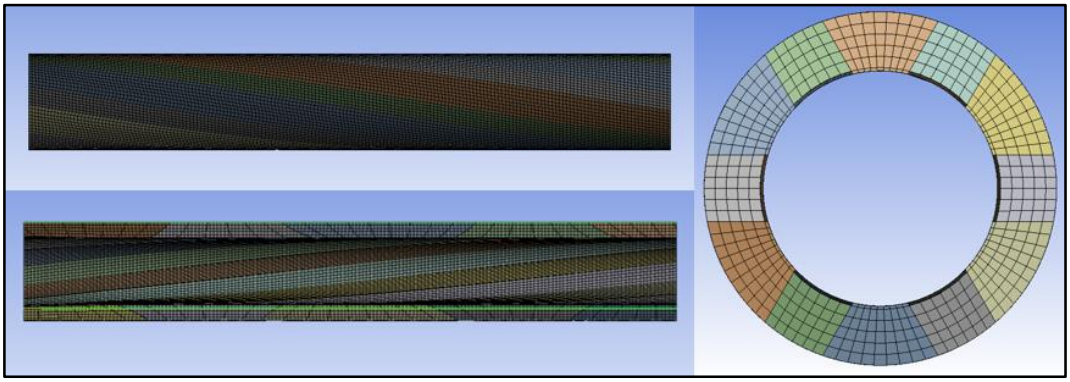

Figure 4. Barrel FE mesh model.

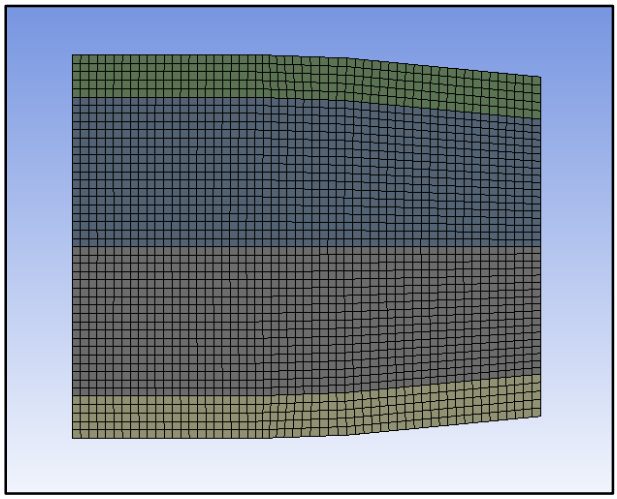

Figure 5. Bullet FE mesh model.

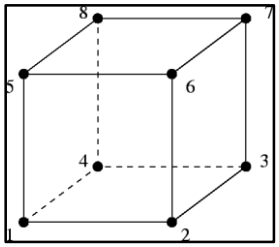

Figure 6. Linear hexahedral element

2.2.4. Boundary conditions and forces

In the barrel analysis model, the left end surface of the barrel shown in Figure 7 is fixed. This means that there will be no displacement in any direction for the selected surface.

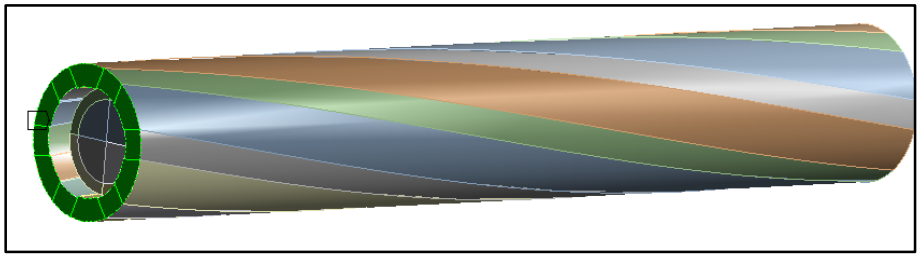

Figure 7. Barrel fixed surface

The pressure obtained from the internal ballistic equations was applied to the rear surface of the bullet in a manner that varied with time, as shown in Figure 8. The graph of this pressure applied to the rear surface of the bullet is shown in Figure 9.

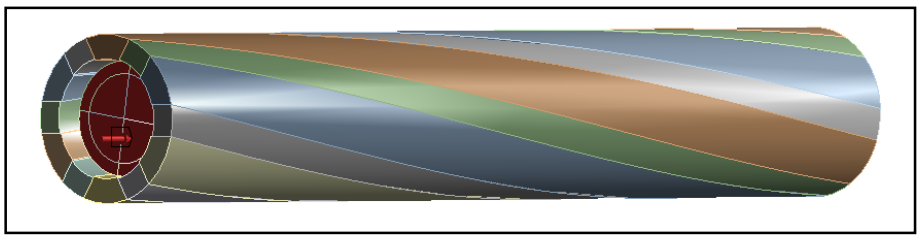

Figure 8. Bullet pressure application surface

The internal ballistic data were obtained using the Vallier-Heydenreich method based on experimental data tables [17].

In Eq. 3, the pressure ratio (η) is shown, where P_{avg} represents the average pressure formed inside the barrel during firing and P_m represents the maximum pressure inside the barrel.

$$\eta = \frac{P_{avg}}{P_m} \tag{3}$$

The bullet path (S_m), time (t_m) and velocity (V_m) at the moment when the gas pressure given in Eq. 4-6 is at its maximum can be calculated using the ballistic factors dependent on the pressure ratio in Table 3.

$$S_m = L \cdot \Sigma(\eta) \tag{4}$$

$$t_m = \frac{2 \cdot L \cdot \Theta(\eta)}{V_0} \tag{5}$$

$$V_m = V_0 \cdot \Phi(\eta) \tag{6}$$

Table 3. Heydenreich ballistic table

η	Σ (η)	θ(η)	Φ(η)	Π(η)	T(η)
0.20	0.0262	0.150	0.322	0.274	0.744
0.25	0.0360	0.196	0.337	0.306	0.792
0.30	0.0471	0.246	0.352	0.338	0.842
0.35	0.0597	0.300	0.367	0.368	0.893
0.40	0.0740	0.358	0.383	0.400	0.946
0.45	0.0903	0.420	0.399	0.432	1.000
0.50	0.1090	0.487	0.416	0.465	1.056
0.55	0.132	0.560	0.435	0.501	1.116
0.60	0.160	0.642	0.457	0.541	1.180
0.65	0.192	0.734	0.482	0.585	1.249
0.70	0.231	0.835	0.511	0.635	1.322
0.75	0.283	0.958	0.546	0.697	1.406
0.80	0.360	1.115	0.592	0.779	1.507

The time the bullet spends in the barrel (t_0) and the gas pressure at the muzzle (P_0) are calculated according to the experimental ballistic factors $T(\eta)$ and $\Pi(\eta)$ in Eq. 7-8.

$$t_0 = \frac{2 \cdot L \cdot T(\eta)}{V_0} \tag{7}$$

$$P_0 = P_{avg} \cdot \Pi(\eta) \tag{8}$$

After determining the bullet position at maximum pressure, the λ parameter given in Eq. 9, which is related to the position of the bullet at any given moment, is determined.

$$\lambda = \frac{S}{S_m} \tag{9}$$

Using the experimental data table of the Vallier-Heydenreich method, the pressure, velocity and time at any position in Eq. 10-12 can be determined with the help of the variables Ψ(λ), Φ(λ) and δ(λ) dependent on the parameter λ. Table 4 shows the weapon information required for the Vallier-Heydenreich method.

$$P = P_m \cdot \psi(\lambda) \tag{10}$$

$$V = V_m \cdot \varphi(\lambda) \tag{11}$$

$$t = t_m \cdot \delta(\lambda) \tag{12}$$

Table 4. Pistol parameters

Barrel length (L, mm)	86
Maximum pressure (P_m, MPa)	230
Bullet initial velocity (V_0, m/s)	350
Powder mass (m_p, g)	0.325
Bullet Mass (M, g)	8
Bullet Diameter (D, mm)	9

The average pressure was calculated using Eq. 13 with the information given in Table 4. Thus, the pressure-time graph showing the pressure change over time required in Figure 9 was obtained.

$$P_{avg} = 2 \cdot \left(\frac{M + ½ \cdot m_p}{L \cdot \pi \cdot D^2} \right) \cdot V_0^2 \tag{13}$$

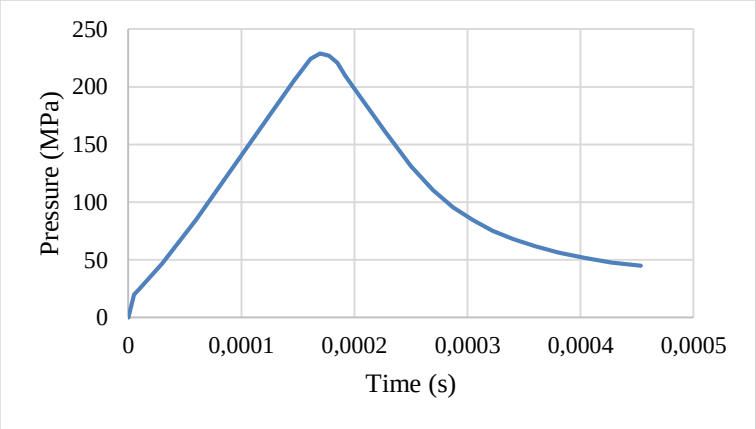

Figure 9. Pressure changes over time

2.2.5. Initial velocity test method

In order to verify the analysis results, the bullet muzzle velocity obtained from the finite element model was compared with the muzzle velocity obtained from the test data. The experimental measurements were carried out in accordance with the TOP 3-2-045/4.1 Initial Inspection Test Standard. Within this scope, three pistols were selected and their serial numbers were recorded. The selected pistols were mounted on firing stands in order and made ready for firing, and then a maximum of ten test shots were fired with each pistol for the calibration of the velocity measurement device and the stand system. During the actual velocity measurements, twelve shots were fired with each pistol, and the bullet velocities at a distance of 10 metres were measured and recorded. After the highest and lowest values were removed from the measurement results, the average value of the remaining ten shots was taken to determine the muzzle velocity for each pistol. The test setup is shown in Figure 10.

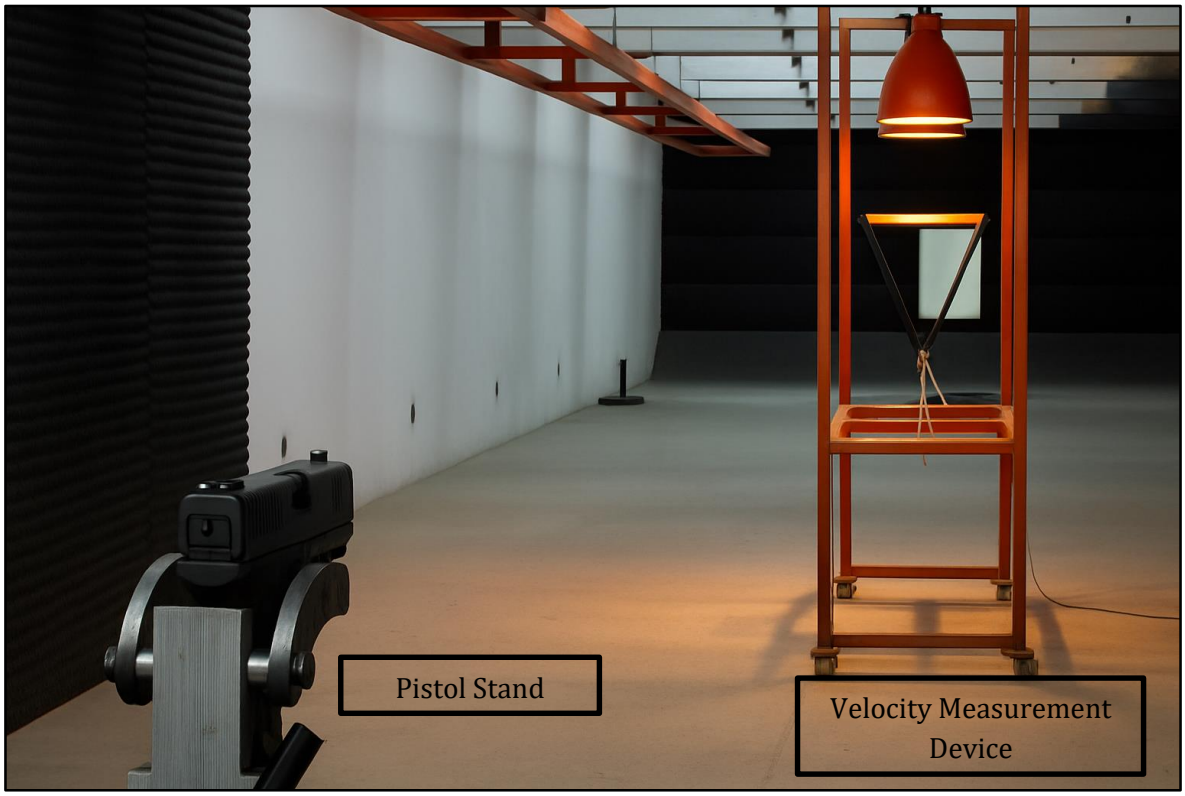

Figure 10. Speed measurement test setup

3. Results

The effects on the barrel and bullet resulting from the firing of a 9 mm calibre pistol were examined through analysis. In order to verify the accuracy of the analysis results, the muzzle velocity obtained from the analysis results was compared with the muzzle velocities obtained from the experimental results. The muzzle velocity obtained from the analysis results was 349.58 m/s, as shown in Figure 11. The muzzle velocity results for three different serial numbers of pistols obtained from the experimental results are given in Table 5. The muzzle velocity values for pistols with serial numbers 15, 21, and 22 are 344, 345, and 341 m/s, respectively. The average muzzle velocity obtained from the experimental shots was calculated as 343.33 m/s, with a standard deviation of 2.81 m/s, indicating a consistent and repeatable firing performance under the test conditions. The deviation between the numerically predicted muzzle velocity (349.58 m/s) and the experimental average (343.33 m/s) is only 1.82%, indicating a high degree of correlation and validating the numerical model.

Figures 11 and 12 show the velocity and position of the bullet over time. When examining the velocity graph of the bullet, it can be seen that the bullet's velocity is very slow up to approximately 100 µs; however, after 100 µs, the velocity value increases significantly (accelerates). In other words, a significant portion of the bullet's initial internal ballistic energy is expended on the plastic deformation of the bullet as it becomes compressed between the lands. After marks form on the bullet's outer surface due to compression by the lands, the bullet accelerates and travels through the barrel.

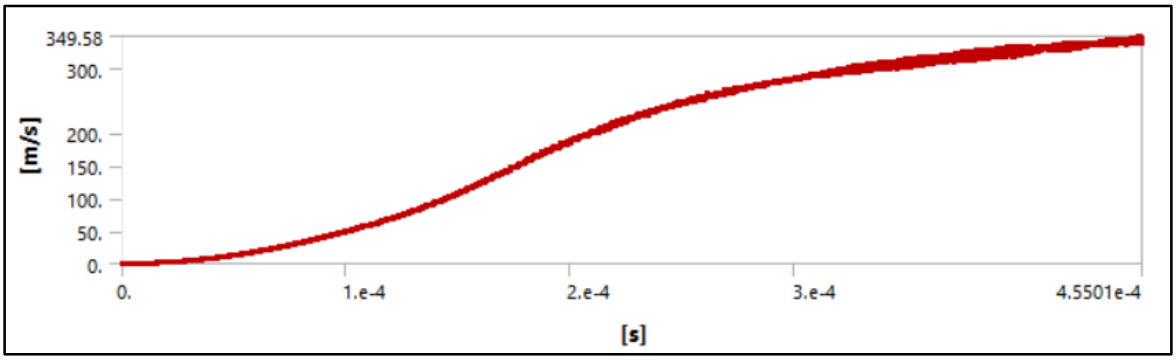

Figure 11. Bullet velocity-time graph

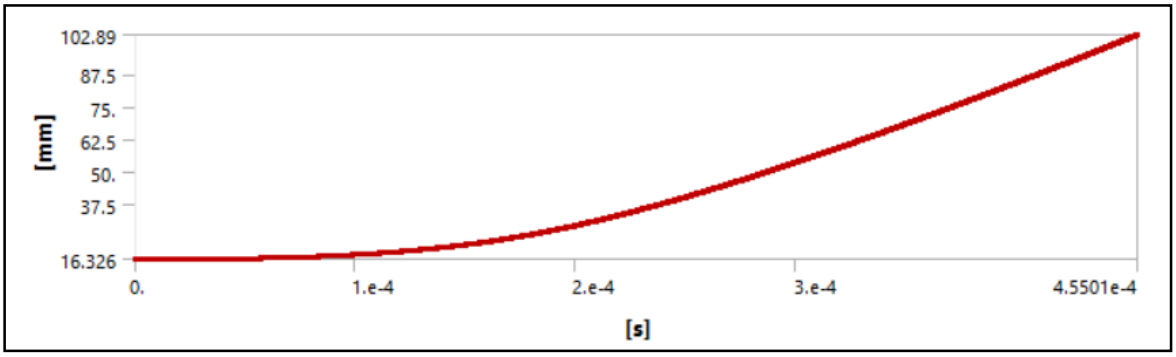

Figure 12. Bullet location-time graph

Table 5. Barrel exit velocity experiment results

Pistol 15	**Pistol 21**	**Pistol 22**
340 m/s	347 m/s	345 m/s
343 m/s	344 m/s	341 m/s
344 m/s	348 m/s	354 m/s
349 m/s	340 m/s	341 m/s
337 m/s	350 m/s	342 m/s
356 m/s	340 m/s	345 m/s
348 m/s	354 m/s	340 m/s
346 m/s	341 m/s	338 m/s
343 m/s	349 m/s	343 m/s
341 m/s	342 m/s	336 m/s
346 m/s	344 m/s	339 m/s
347 m/s	349 m/s	341 m/s
AVG 344 m/s	**AVG 345 m/s**	**AVG 341 m/s**

The movement of the bullet inside the barrel at t=0 µs, t=75 µs, t=150 µs, t=225 µs, t=300 µs, t=375 µs and t=455 µs is shown in Figure 13 as A, B, C, D, E, F and G, respectively.

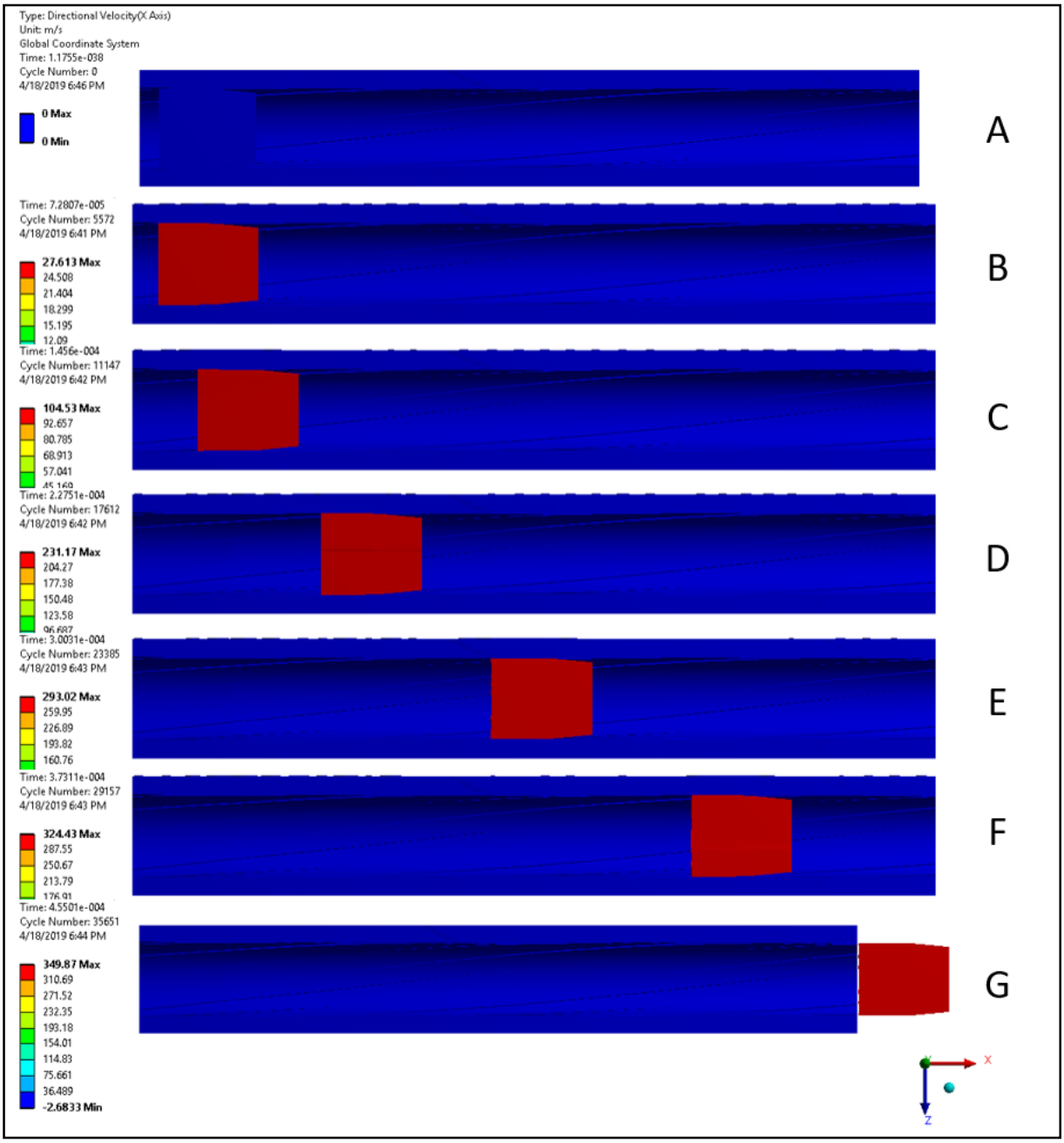

Figure 13. Bullet movement inside the barrel at various time steps (t=0–455 μs)

The equivalent stress, which can also be expressed as the von Mises stress formed in the barrel, is given in Figure 14 as A, B, C, D, E, F and G for t=0 μs, t=75 μs, t=150 μs, t=225 μs, t=300 μs, t=375 μs and t=455 μs, respectively. Additionally, the time-dependent variation of the equivalent stress is shown in Figure 15.

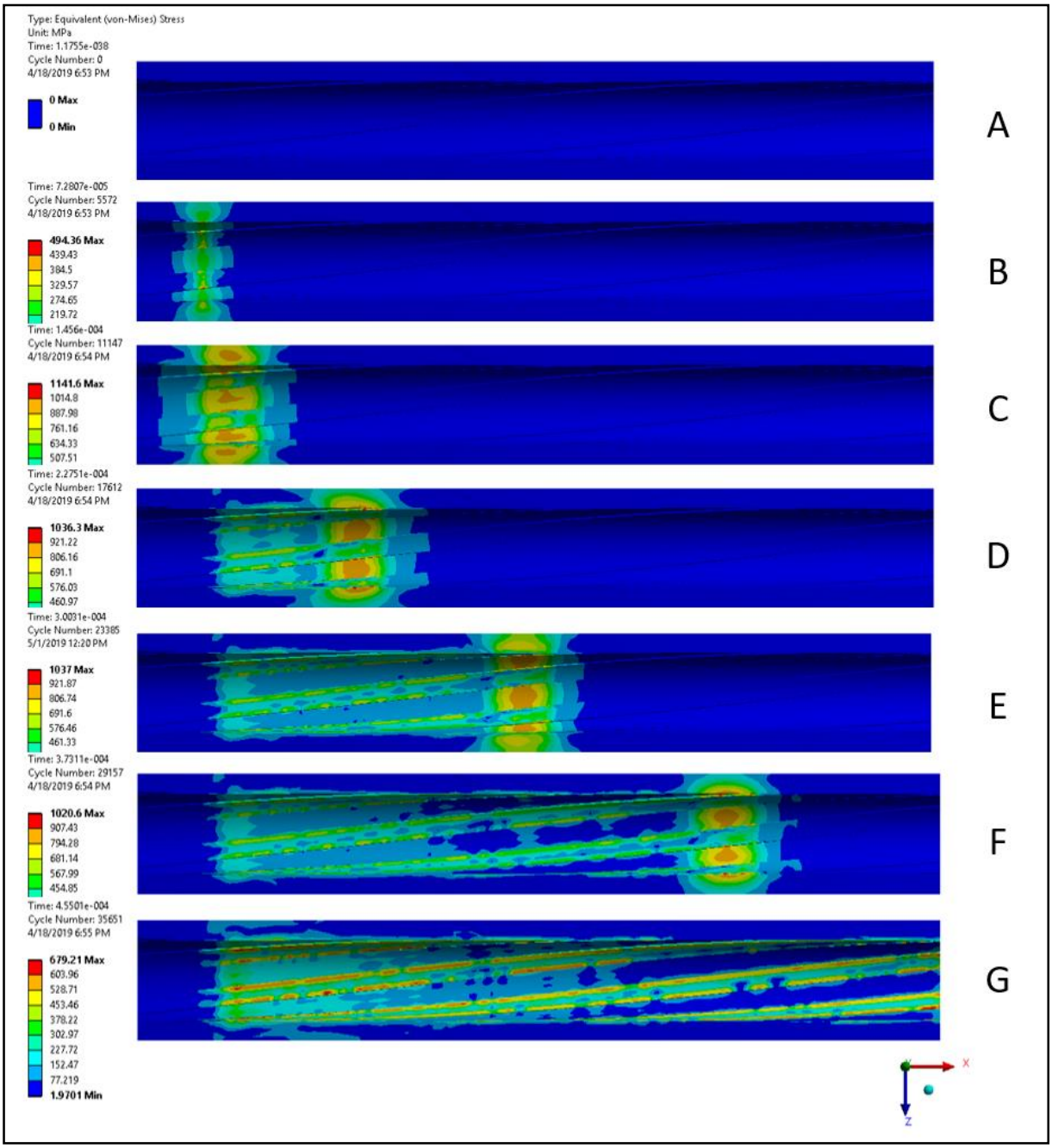

Figure 14. Time-dependent evolution of maximum equivalent von Mises stress in the barrel

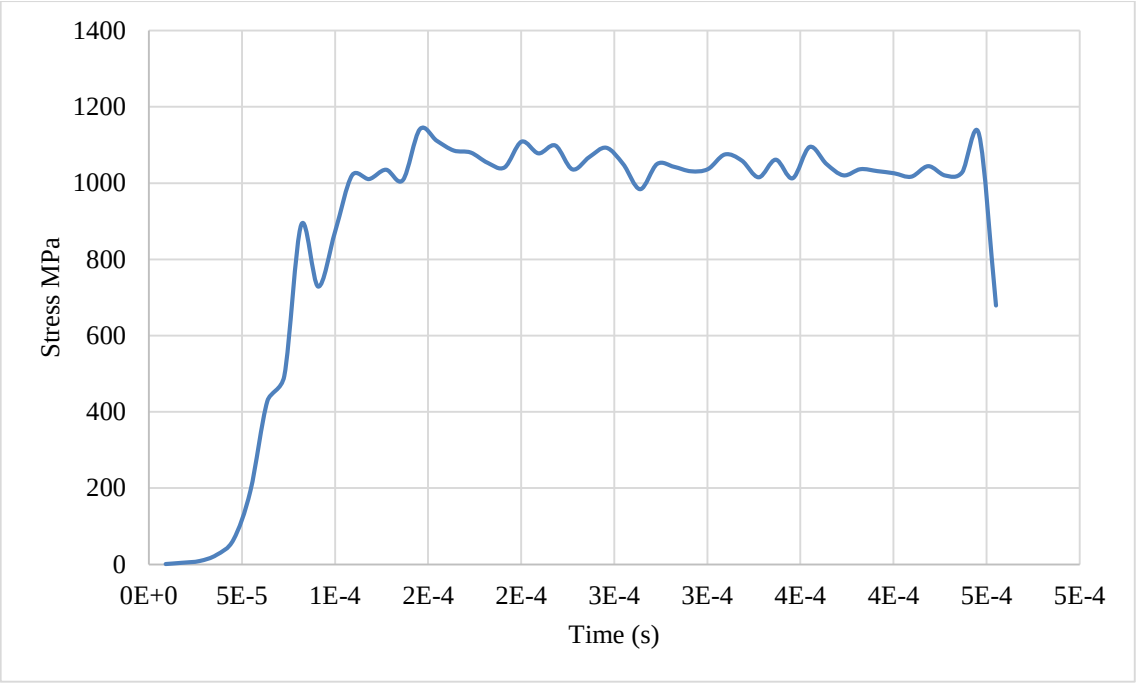

Figure 15. Change in maximum equivalent stress over time

This equivalent stress value obtained is the maximum equivalent stress generated during the movement of the bullet and occurs in the grooves. The equivalent stress value generated in the barrel grooves is 1141.6 MPa for a maximum t=146 µs (Figure 18), the equivalent stress value formed in the grooves is 942 MPa at t=209 µs (Figure 16), and the maximum equivalent stress formed on the outer surface of the barrel is approximately 938 MPa at t=154 µs (Figure 17).

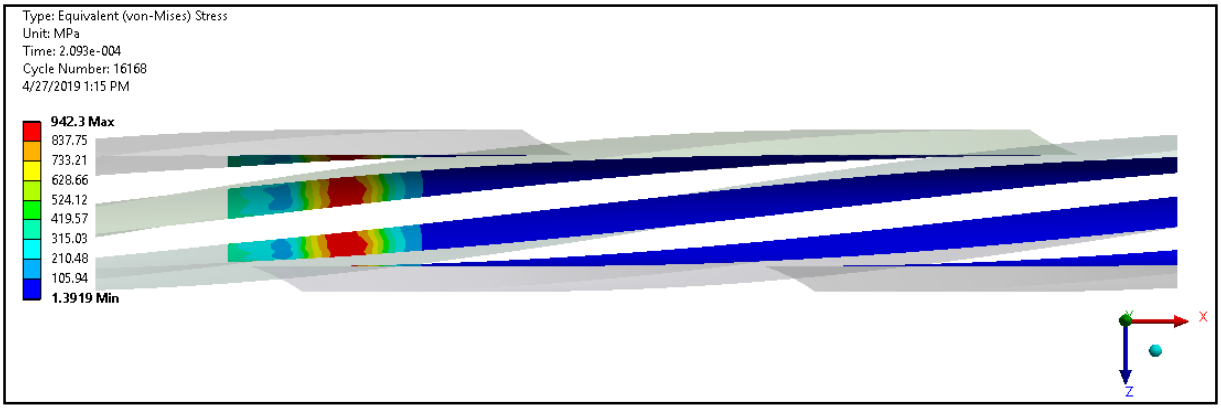

Figure 16. Maximum equivalent stress formed in the grooves (t=209 µs)

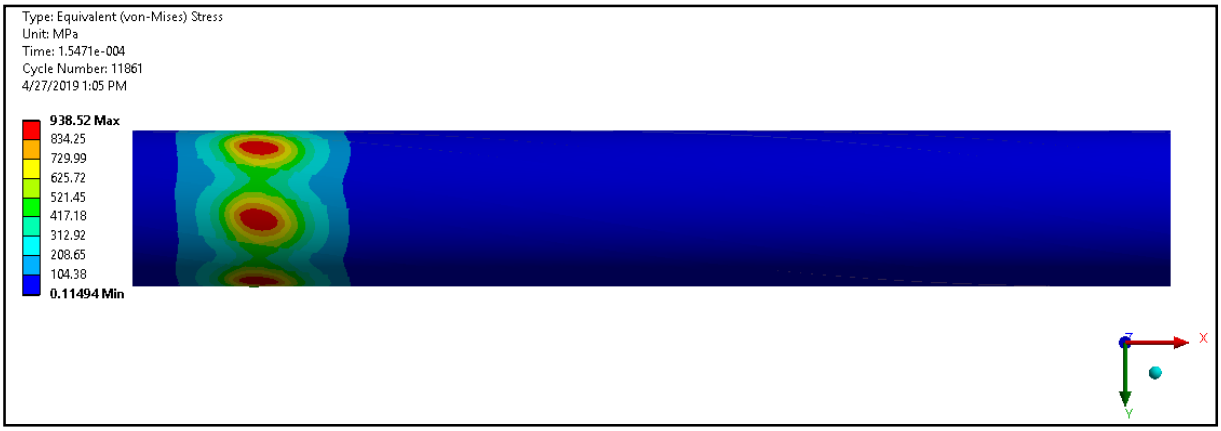

Figure 17. Maximum equivalent stress formed on the outer surface of the barrel (t=154 µs)

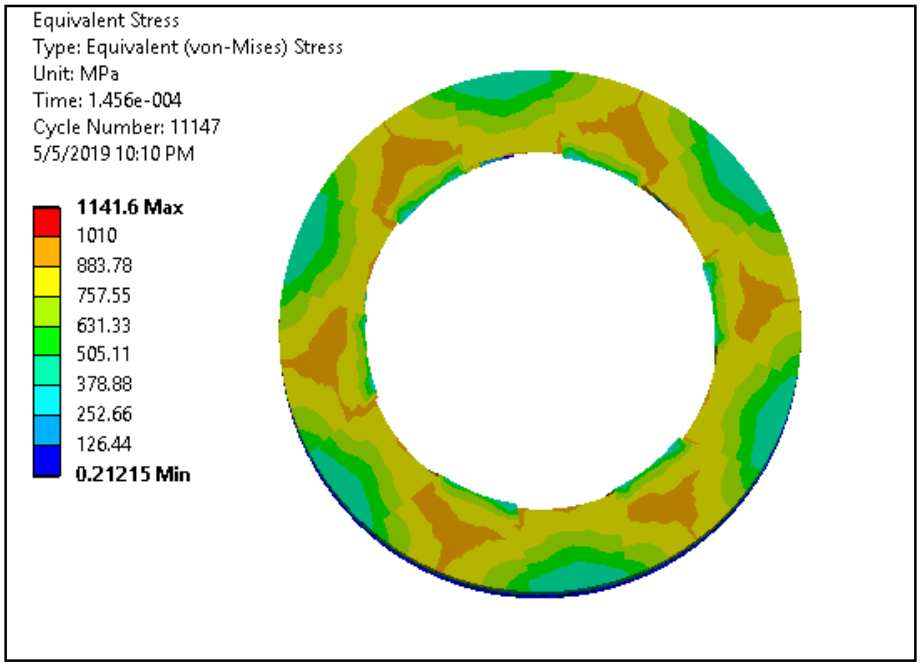

Figure 18. Maximum equivalent stress formed in the barrel section (t=146 μs)

When examining the equivalent stress formed in the barrel section shown in Figure 18 (t=146 μs), it can be seen that the yield stress (1010 MPa) is concentrated in a very small local area. As seen in Figure 19, the maximum equivalent stress occurs at the sharp corners of the grooves, and the stresses around this region are below the yield stress.

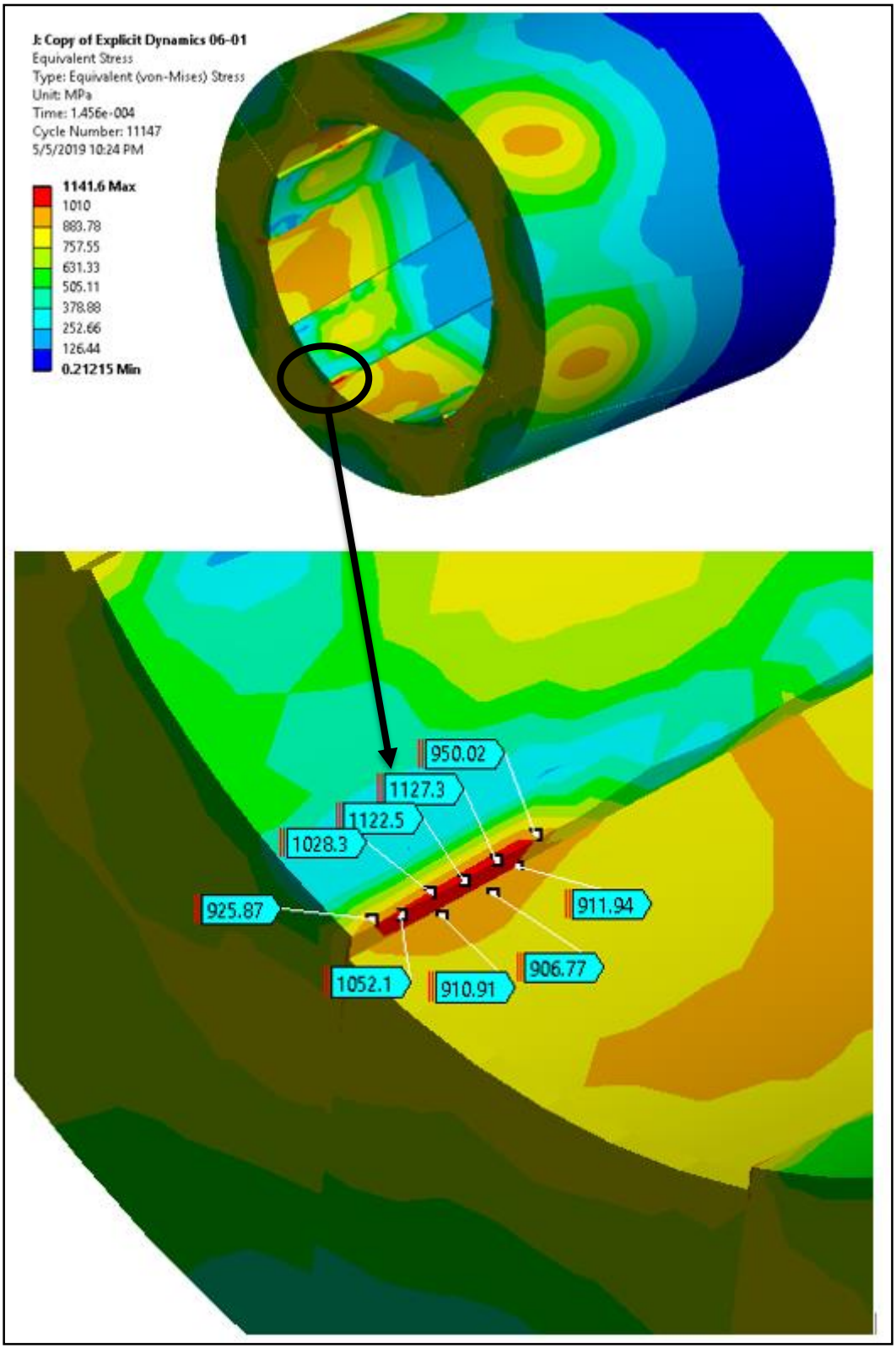

Figure 19. Local stress region formed in the grooves.

As a result of the pressure exerted by the grooves on the bullet, the bullet material has undergone plastic deformation. The maximum amount of plastic deformation in the bullet is 0.27, as shown in Figure 20. Figure 21 shows the plastic deformation that occurs during the bullet's movement inside the barrel. The symmetrical distribution of plastic deformation is a result of the bullet interacting smoothly with the inner wall of the barrel.

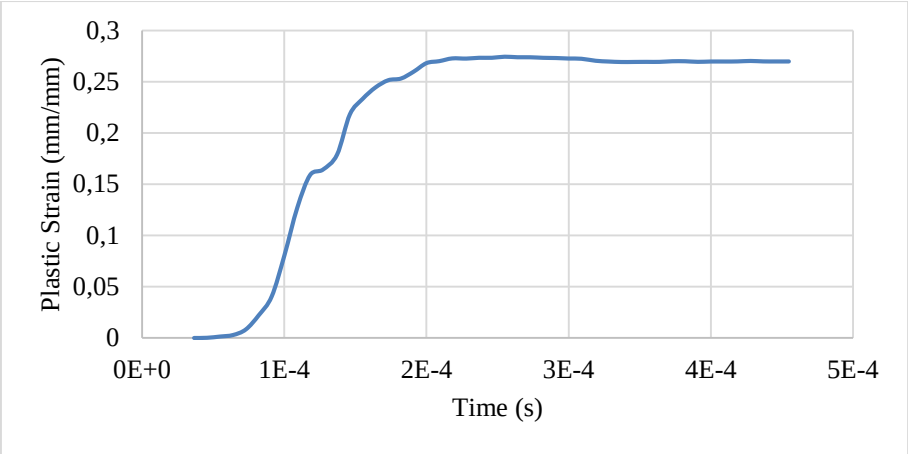

Figure 20. Time-dependent change in equivalent plastic deformation on the bullet

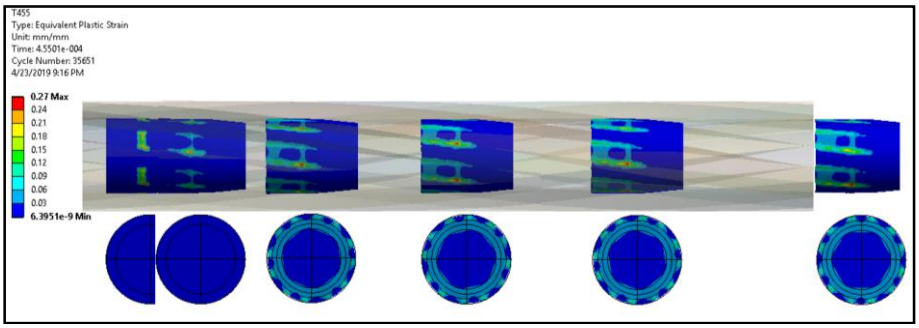

Figure 21. The equivalent amount of plastic deformation generated during the movement of the bullet inside the barrel

The range shown in Figure 22, where the strain rate is at its maximum, covers the area where plastic deformation and stress are at their highest.

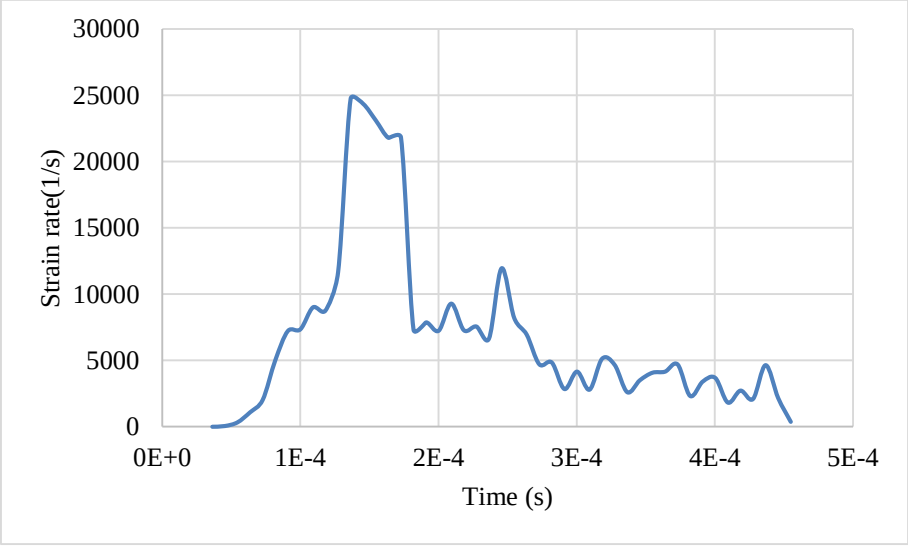

Figure 22. The strain rate that occurs during the movement of the bullet inside the barrel

After the test, the deformed bullet geometries were scanned using 3D scanning methods and STL files were obtained. The surface sample obtained from this scan is shown in Figure 23. The deformed geometry was compared with the actual geometry by taking a cross-section from a plane 2 mm away from the bullet base, and the amount of deformation on the radial axis was measured as a maximum of 0.122 mm, as shown in Figure 24. As a result of the analyses performed using FEA, the deformed bullet core was compared with the original bullet core, and the maximum deformation was measured as 0.111 mm, as shown in Figure 25. When the tests and analyses were compared, the difference between them was calculated as 0.011 mm.

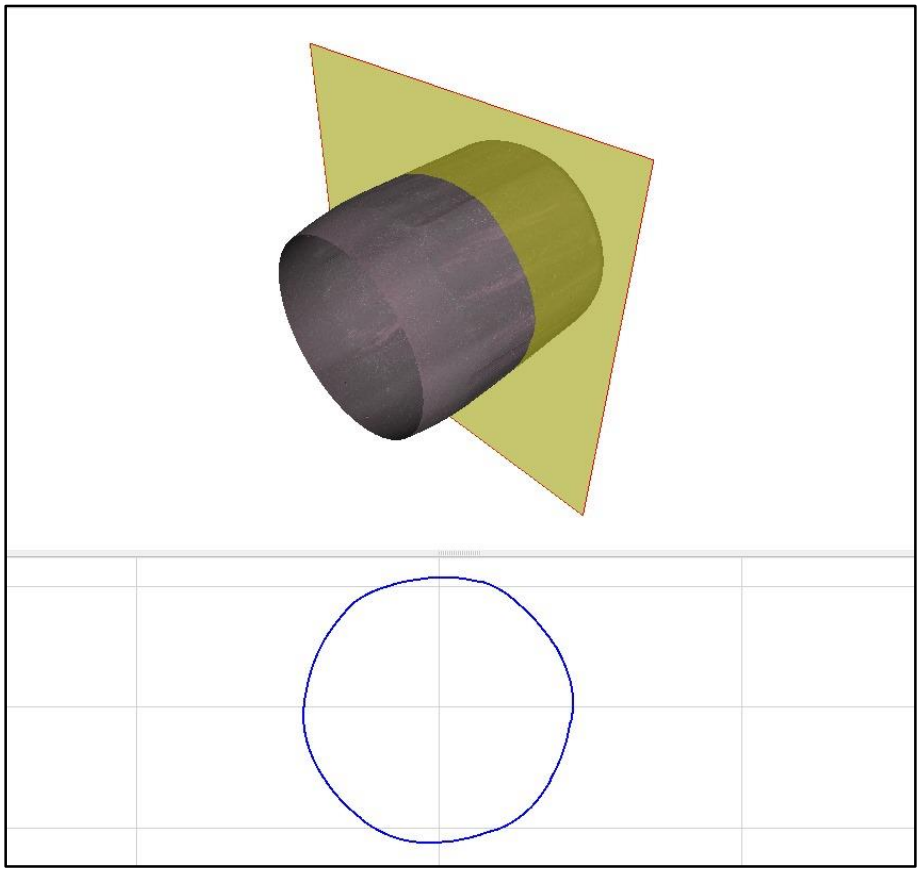

Figure 23. Scanned Bullet Core and Cross-Section

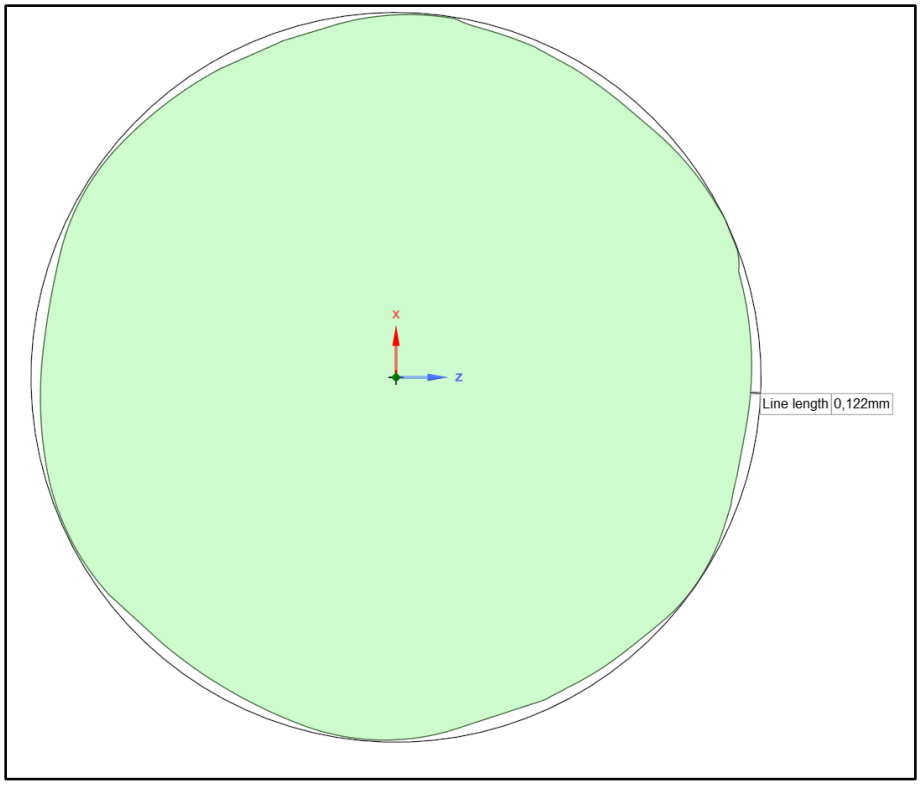

Figure 24. Comparison of the deformed bullet section with the undamaged initial bullet section as a result of the tests conducted

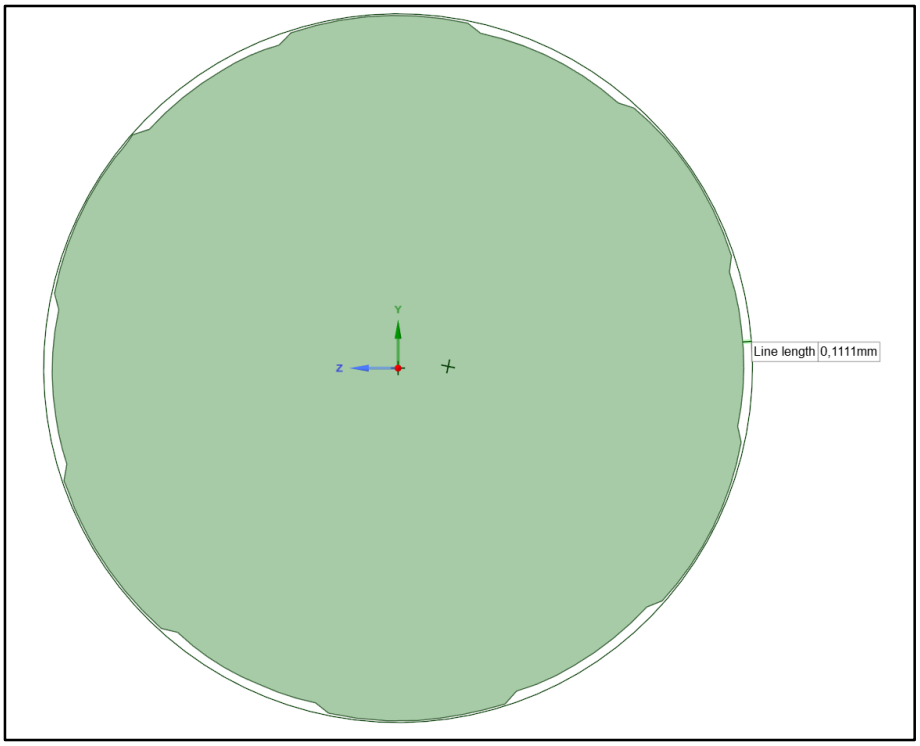

Figure 25. Comparison of the deformed bullet section with the undamaged initial bullet section as a result of the analyses performed

4. Discussion and Conclusion

In this study, the internal ballistic process in a 9x19 mm calibre pistol barrel was successfully modelled using the finite element method (FEM), and the numerical analysis results were verified with experimental data. The primary objective of the study was to develop a numerical model capable of reliably predicting the complex thermomechanical behaviours such as stress, plastic deformation, and velocity that occur between the barrel and the bullet during firing.

The bullet muzzle velocity, which is the most critical parameter in the validation of the analysis results, was used as the primary indicator of the model's validity. As a result of the numerical analysis, the bullet muzzle velocity was calculated as 349.58 m/s. This value shows a deviation of 1.82% when compared to the average muzzle velocity of 343.33 m/s obtained from experimental shots fired with three different pistols. This high degree of agreement between numerical and experimental results demonstrates the overall accuracy of the model and its ability to represent the internal ballistic process.

The physical accuracy of the model is further reinforced by comparing the plastic deformation that occurs in the bullet after firing. Bullets examined using 3D scanning after actual firing showed a maximum deformation of 0.122 mm in the radial axis. The finite element analysis (FEA) predicted this deformation to be 0.111 mm. The minimal deviation of 0.011 mm between experimental and numerical deformations highlights the model’s capability to accurately predict mechanical response during bullet-barrel interaction, validating both geometric fidelity and material behaviour.

The analyses revealed that the bullet's velocity was quite slow in the initial moments of its movement (up to approximately 100 μs), during which a significant portion of the internal ballistic energy was expended on plastic deformation as the bullet became wedged into the rifling and lands. Acceleration was observed to begin once the bullet had fully seated itself into the rifling and lands. Stress analysis in the barrel showed that, as expected, the highest stress (1141.6 MPa) occurred when the bullet applied pressure to the sharp corners of the rifling and lands. Although this stress value exceeded the yield stress (1010 MPa) of the barrel material, AISI 4340 steel, in an instantaneous and very small local area, it was understood that this did not threaten the overall structural integrity of the barrel.

In this study, certain geometric simplifications were applied to the bullet and barrel models in order to reduce computational complexity and meshing effort. For instance, small fillets, chamfers, and the rounded nose of the bullet were omitted, and sharp transitions were used in several contact regions. While these simplifications significantly improve simulation efficiency, they may also result in local stress concentrations, particularly near sharp corners and contact interfaces. Although a quantitative comparison between simplified and fully detailed geometries was not conducted within the scope of this study, the observed consistency between the numerical and experimental results in terms of muzzle velocity and deformation suggests that the global mechanical response of the system remains reliably captured. Nonetheless, the potential impact of these simplifications on local stress predictions is acknowledged as a limitation, and future work may involve detailed geometry-based validation for enhanced accuracy in local mechanical behaviour.

Within the scope of this research, simplifications were made to the barrel and bullet geometries to optimise the calculation time, and the gas pressure generated by the combustion of the propellant was applied to the model as a pressure-time curve obtained using the Vallier-Heydenreich equations, rather than a direct fluid-solid interaction simulation. Despite these simplifications, the high degree of agreement between the obtained results and experimental data demonstrates the effectiveness of the developed methodology.

In conclusion, this study demonstrates that experimentally validated finite element models are a powerful and efficient tool for reducing prototype dependency and development costs in the design and optimisation of firearm systems. The proposed model provides a reliable foundation for evaluating the effects of various parameters such as barrel materials, rifling geometries, and ammunition characteristics on ballistic performance and barrel longevity. In future work, the current model could be further enhanced by incorporating a more detailed representation of propellant gas behaviour through Computational Fluid Dynamics (CFD) simulations. Although fluid–solid interaction models such as CFD offer greater insights into gas expansion and thermal effects, their implementation was beyond the scope of this study due to computational and modelling constraints. Nevertheless, integrating coupled CFD-FEM approaches remains a promising direction for achieving a more comprehensive simulation of the internal ballistic process.

References

[1] Morphy,C.C, Fisher,E.B, "*The Role Carburization In Gun Barrel Erosion And Cracking*",Technical Library AD-A102625, (1981).

[2] Özcan, H. (2012). *32CrMoV çeliğinin aşınma direncini arttırmak için yeni bir ısıl işlem metodunun geliştirilmesi* [Master's thesis, Hacettepe University].

[3] Değirmenci, E. (2010, December). *Yüksek sıcaklığa ve dinamik iç basınca maruz kompozit destekli boru tasarımı* [Doctoral dissertation, Kırıkkale University].

[4] Piticari, I.-L., Pirlot, M., Sava, A. C., & Vanhove, A. (2015). The influence of muzzle devices over bending vibrations of an automatic rifle barrel. Revista Academiei Forţelor Terestre, 3(79), 381–388.

[5] Zhang, Y., Jia, Z. (2011). Dynamics simulation of floating automatic rifle. 2011 Second International Conference on Mechanic Automation and Control Engineering, Inner Mongolia.

[6] Nelson, C. W., & Ward, J. R. (1981). *Calculation of heat transfer to the gun barrel* (Memorandum Report ARBRL-MR-03094).

[7] Huang, C. J. (1993, October*). Transient stress and failure analysis of 105 mm gun barrel caused by projectile premature* [Master's thesis, Lehigh University].

[8] Deng, S., Sun, H.K.,"Transient Finite Element For İn-Bore Analysis Of 9 mm Pistol", Applied Mathematical Modelling , Volume 38,Issues 9-10 (2013).

[9] Sönmez, U. (2009, June). *Obüs namlusu yanma odasında atış esnasında ortaya çıkan gerilmelerin matematiksel modellenmesi ve analizi* [Master's thesis, Sakarya University].

[10] Öztürk, Y. F. (1999). *Hesaplamalı akışkanlar dinamiği (HAD) yöntemiyle namlu analizi* [Master's thesis, İstanbul University].

[11] Akçay, M., & Yükselen, A. (2014). Unsteady thermal studies of gun barrels during the interior ballistics cycle with non-homogenous gun barrel material thermal characteristics. *Thermal Science and Technology*, *34*(2), 75–81.

[12] Daniş, F. (2014). *Ballistic simulation software development for solid propellant guns* [Master's thesis, Middle East Technical University, Graduate School of Natural and Applied Sciences].

[13] Gündüzer, O. (2011, November). *Namlu cidarı boyutlandırılmasına iç balistik davranışın etkisi* [Master's thesis, Gazi University].

[14] Tawfik, M. (2008). Dynamics and stability of stepped gun barrels with moving bullets. *Advances in Acoustics and Vibration*, 1–7.

[15] Stiavnicky, M., & Lisy, P. (2013). Influence of barrel vibration on the barrel muzzle position at the moment when bullet exits barrel. *Advances in Military Technology*, *8*(1), 89–102.

[16] Ansys Inc. (2018). *Ansys theoretical manual* (Version 19.2).